



# EDFA Controlled Spectral Efficient MIMO Free Space Optic Links for Mitigation of Climatic Turbulence Conditions

Yogesh Kumar Gupta<sup>1</sup> · Aditya Goel<sup>1</sup>

Accepted: 31 August 2023 / Published online: 9 October 2023

© The Author(s), under exclusive licence to Springer Science+Business Media, LLC, part of Springer Nature 2023

## Abstract

Free space optical communication (FSO) employs an optical setup to transmit the message signal directly through the air from the source to the receiver. While FSO offers several advantages, its effectiveness for long-distance transmission is hindered by the impact of climate change and pointing error. To address this challenge, this study focuses on improving the efficiency of FSO systems in terms of channel capacity and long-distance communication. To achieve this objective, a 32-channel wavelength division multiplexing (WDM) FSO approach, along with pre- and post-amplification techniques using erbium-doped fiber amplifier (EDFA), and a multiple-input multiple-output (MIMO) technique, have been employed. Furthermore, the proposed framework is evaluated using various modulation schemes, such as gaussian pulse generator (GA), return to zero (RZ), and non-return to zero (NRZ). The proposed system has achieved a channel capacity of 320 Gbps. The proposed system achieves extended transmission ranges: 35 km under clear conditions, 1.37 km under foggy conditions, and 2.53 km under rainy conditions. Furthermore, we formulate a closed-form expression for the bit error rate (BER) in the MIMO FSO system. The performance is evaluated in terms of BER and quality factor (Q Factor). The proposed system outperforms existing designs in terms of transmission range and spectrum efficiency.

**Keywords** FSO · MIMO · WDM · EDFA · BER · Q Factor

## 1 Introduction

To accommodate the expanding needs of cellular systems, the broadband access market is expanding to new areas based on optical wireless technology. The most common forms of broadband connectivity nowadays are cable and radio frequency (RF) lines. Cable allows for connectivity whatever be the climate, but its point-to-point infrastructure makes the “last

---

✉ Yogesh Kumar Gupta  
yogesh.fetgkv@gmail.com

<sup>1</sup> Department of Electronics and Communication Engineering, Maulana Azad National Institute of Technology, Bhopal, Madhya Pradesh, India

mile” costly [1]. Additionally, RF connections may function in any climate and don’t need a special point-to-point setup. However, the current state of RF technology is problematic due to the aforementioned strong demand and the high cost of necessary licenses.

FSO employs a laser beam in empty space to convey information. FSO surpasses fibre optic technology due to its affordability, compact size, high throughput, and faster transmission rates. With FSO, significant technological advancements are possible and may come sooner rather than later. The signal received by the receiver deteriorates due to air turbulence. Yet, spatial distinguishing quality methods had made it feasible to lessen the optical signal’s impact on the surrounding environment in FSO setups [2–4]. The system efficiency had been enhanced in numerous difficult circumstances thanks to the FSO framework’s use of spatial diversity. Higher-order diversities was illuminated by increasing the Q Factor. These methods aid in making FSO operations more effective [5]. Mai Banawan et al. [6] employed the integration of WDM and MIMO techniques to augment the channel capacity. Figure 1 depicts the basic framework of the FSO link. Digital information is processed with a continuous wave laser. After modulation, this optical signal is transmitted through the FSO channel. In the receiver part, the photodetector (PD) detects this signal. A low-pass filter (LPF) is employed in the signal to eliminate undesirable background noise. The performance of this system is evaluated by the BER tester.

To conduct the performance analysis of the FSO system, a variety of modulation schemes were used. B. Sridhar et al. [7] demonstrated the performance of the FSO system based on different modulation techniques, investigating various types of channel instabilities including rain, fog, physical blockage, scintillation, and more. Performance metrics were analyzed using the Gamma-Gamma approach in [8], helping understand the intensity of optical channels. R. Nebuloni et al. [9] investigated fog-induced attenuation in FSO systems, deriving the relationship between fog’s extinction coefficient and visibility. Moreover, uncertainties arising from microphysics and visibility measurement methods were assessed for their impact on FSO power budgets. Xiaozong Yu et al. [10] employed the performance of dual-hop FSO system considering atmospheric turbulence, absorption, and pointing errors. Furthermore, this investigation [10] formulated precise expressions for the outage probability and average BER (ABER) using various detection techniques. Moreover, to obtain the results, the distance of the single FSO and dual-hop FSO link was considered to be 1800 m and 900 m respectively. Guanjun Xu et al. [11] investigated unmanned aerial vehicles (UAV)-assisted dual-hop FSO systems on the basis of attenuation loss, atmospheric turbulence, pointing

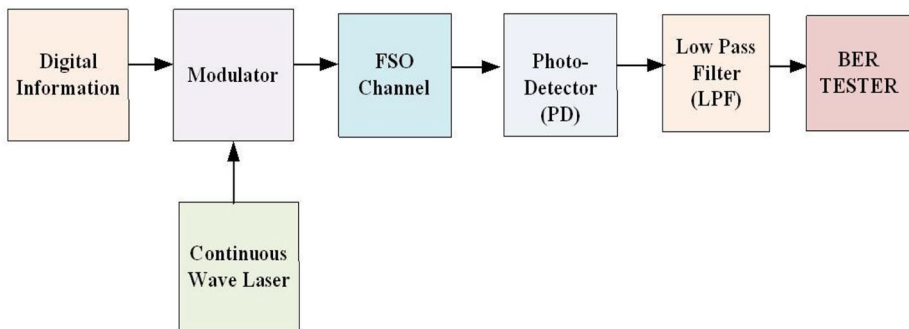


**Fig. 1** Basic architecture of the FSO module

errors, and angle-of-arrival fluctuation. Moreover, this paper [11] derived the expression of outage probability and ABER. Furthermore, in order to achieve the results, the distances for the source-to-UAV and UAV-to-destination links were set at 20 km and 3 km, respectively. The simulation results of this research [11] also indicated that foggy weather severely hampered the transmission of the FSO system and led to an increase in the BER.

Anuranjana et al. [12] proposed the integration of mode division multiplexing (MDM), WDM, and FSO systems under foggy conditions. Ekta Vasani et al. [13] employed the spectrum slicing wavelength division multiplexing (SS-WDM) technique with the FSO system. The transmission range achieved in this paper [13] was 1–5 km. The performance of the FSO system was analyzed using the aperture averaging method in [14]. Ekta Vasani et al. [15] discussed the integration of SS-WDM and polarization division multiplexing techniques with the FSO system, examining the system's performance under various atmospheric conditions, including rain, fog, snow, and others. Ebrahim E. Elsayed et al. [16] examined the utilization of dense wavelength division multiplexing for transmission within an integrated FSO system, employing on-off Keying and digital-pulse position modulation. This work [16] achieved a data rate of 2.5 Gbps on each channel. Mehtab et al. [17] evaluated the effectiveness of the FSO system based on orbital angular momentum (OAM) schemes using RZ, NRZ, and alternate mark inversion modulation schemes. According to the findings of this study [17], NRZ modulation schemes provide superior outcomes compared to RZ modulation schemes and other mark-inversion modulation schemes. Additionally, they were able to achieve a data throughput of 40 Gbps. Lamia et al. [18], in various climates, used the Spectral Amplitude code division multiple access method to perform a performance study of the FSO system. This article [18] employed NRZ modulation schemes and achieved a data rate of 1 Gbps. H. Singh et al. [19] employed the integration of a  $16 \times 10$  Gbps WDM system with orthogonal frequency division multiplexing technique to analyze the performance of the FSO system. Furthermore, in coastal areas where the attenuation was 0.5 dB/km the highest transmission range the BER achieved in this study [19] was 10.75 km and  $10^{-9}$ , respectively. Investigating the functionality of the FSO system, Farouk et al. [20] utilized  $2 \times 2$  FSO transceiver modules, revealing that the achievable transmission range ranged from 1.6 to 3.9 km. N. Rani et al. [21] proposed a  $4 \times 4$  FSO transceiver module, with their study indicating that the achievable transmission range via direct detection was approximately 4.5 km. To enhance the functionality of the FSO link, our previous work [22] employed a hybrid combination of multiple beams and the WDM approach. The findings presented in this study [22] demonstrate improved channel capacity and spectral efficiency. For the simulations in this study [22], we exclusively considered clear climatic conditions.

## 1.1 Research Gaps and Main Contributions

The state-of-the-art literature studies show the different methods employed for mitigating atmospheric turbulence, environmental conditions (rain, fog) and pointing error problems in the FSO framework. Yet, these approaches fell short of achieving satisfactory results in terms of maximum transmission range, spectrum efficiency and channel capacity. This study is dedicated to elevating the performance of FSO by boosting channel capacity and enabling long-distance transmission.

This paper presents a suggested architecture for a 32-channel WDM FSO system, utilizing pre- and post-amplification techniques along with direct detection technology. To aid

system architects, a comprehensive simulation framework employing MIMO methods has been developed. The OptiSystem tool was utilized to evaluate this model, which constitutes the primary contributions of this study. Specifically, the contributions are as follows:

- i) We have designed a direct detection-based WDM FSO system that efficiently mitigates the impact of environmental turbulence, including rain, fog, and pointing errors. Furthermore, the model parameters are optimized using a single-parameter optimization (SPO) approach, and the channel component benefits from the utilization of the MIMO technique. Moreover, we have derived the closed-form expression of the BER for MIMO FSO system.
- ii) With the help of a parametric study of the BER and Q Factor, we simulated and analyzed the results.
- iii) Moreover, we compared our outcomes with designs extracted from cutting-edge literature research. This comparison encompassed factors such as transmission range in different climatic conditions (rain, fog), multiplexing techniques, information rates, optimization methods, and the inclusion of pointing error impairments.
- iv) The proposed design outperforms previous research in terms of transmission range and channel capacity, as confirmed by the obtained results.

There are five parts to this study. In the Introductory Part, the value of the FSO connection is examined using the review of relevant literature. In the Sect. 2, “Methodology” we will discuss the architecture of the proposed system design. The parameters and the values that are given in the simulation are discussed in the Sect. 3. We will explore the outcomes of applying the provided framework in the [results and discussion](#) Section. Finally, In the [Conclusion](#) Section, the planned work is ended, and a discussion of the proposed system’s ongoing work is presented.

## 2 Methodology Analysis

The suggested Pre- and Post-amplification-based MIMO WDM FSO framework is illustrated in the block diagram presented in Fig. 2. This section provides a detailed discussion and theoretical analysis of the framework. The creation of the intricate stage process within the framework is examined. In this context, several components are referred to by their abbreviations: “PRBS” denotes the “Pseudo Random Bit Sequence” generator, “Mach-Zehnder modulator” is represented as MZM, “CW Laser” refers to the continuous wave laser, and the power splitter is denoted as PSP. Additionally, the abbreviations used in this study include WDM MUX for wavelength division multiplexer, OA for optical amplifier, PC for power combiner, WDM DEMUX for wavelength division demultiplexer, and 3RG for 3R regenerator.

### 2.1 Transmitting Section

The transmitter part of Fig. 2 involves the generation of random bits by the PRBS for communication purposes. These random bits are then transformed into different waveforms using NRZ, RZ, and GA modulation schemes. On the other hand, the CW laser emits a laser

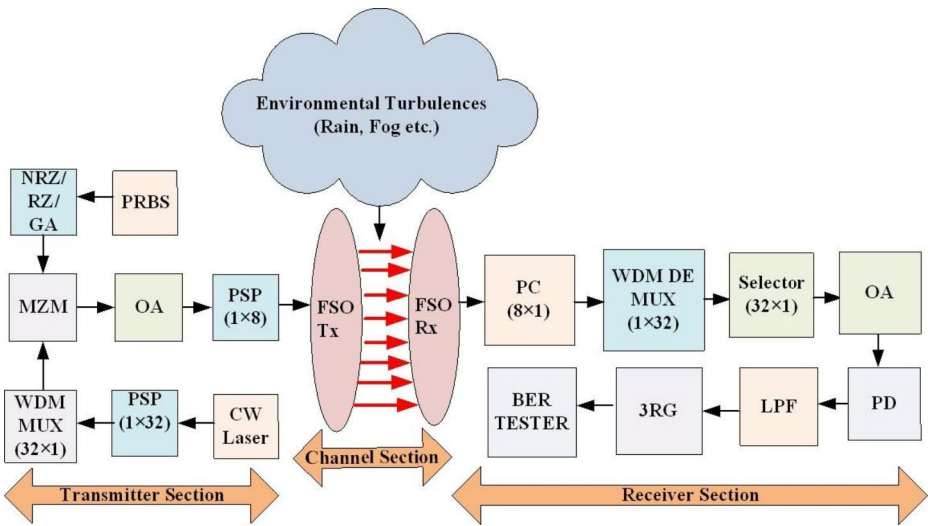


**Fig. 2** Proposed Pre- and Post-amplification-based multiple beam WDM FSO system

beam with a frequency of 193.1 THz. The optical signal is divided into 32 individual output signals by the PS ( $1 \times 32$ ) component. Subsequently, the signal is multiplexed using a WDM MUX ( $32 \times 1$ ). The MZM, working together with the WDM MUX ( $32 \times 1$ ), transforms the electrical signals from the NRZ, RZ, and GA modulation schemes into the optical domain. The OA amplifies the strength of the optical signal. EDFA is utilized in various configurations within this scheme for the purpose of amplification. When the EDFA is positioned at the transmitter side, the receiver side, or both sides, it is denoted as the PRE, POST, and PREPOST-amplification configurations, respectively. The PS ( $1 \times 8$ ) then separates this composite signal into 8 individual output signals. After processing, the optical signal is transmitted through the FSO transmitter (FSO Tx) module over the transmission medium.

## 2.2 Channel Section

In the Channel section, the FSO Tx module transmits 8 beams. The channel experiences various turbulence losses, including scintillation, rain, fog, haze, and dust, among others. Each of these factors uniquely influences the quality of the FSO link signal.

### 2.2.1 Scintillation

Scintillation pertains to rapid variations in the optical signal's intensity and phase due to atmospheric turbulence. This occurrence induces signal fading, resulting in reduced received power and elevated BER. To counteract these effects, techniques like adaptive optics and diversity are combined together to mitigate the impact of scintillation and enhance the system's resilience [8], [23].

### 2.2.2 Rain

Raindrops can absorb and scatter optical signals, which are the leading causes of attenuation and fading of the signal. Shorter wavelength signals experience higher attenuation because rain-induced attenuation is dependent on the wavelength of the signal. Quantifying rain-induced signal degradation involves rain rate and specific attenuation models, and mitigation strategies encompass adaptive power control and link budget optimization [20], [24].

### 2.2.3 Fog

Fog particles scatter and absorb optical signals, causing attenuation and degrading signal quality. Fog-induced attenuation varies based on factors such as fog density, wavelength, and visibility. Longer wavelengths, like 1550 nm, display improved performance in foggy conditions due to reduced scattering [25]. The mitigation of fog-induced degradation is facilitated through advanced modulation schemes and wavelength diversity [12].

### 2.2.4 Haze

Haze, composed of suspended particles and moisture, contributes to optical signal scattering and absorption. The degree of haze-induced attenuation is contingent on particle size, concentration, and wavelength. In hazy environments, signal quality can diminish, resulting in higher BER. The adoption of higher-order modulation schemes and spectral slicing techniques can offset the negative impact of haze [13], [15].

### 2.2.5 Dust

Atmospheric dust particles can attenuate optical signals through both scattering and absorption. Dust-induced attenuation is influenced by particle size, concentration, and wavelength. The presence of dust may lead to signal fading and reduced link quality. Adaptive modulation and coding strategies are viable solutions to counteract the effects of dust-induced degradation [26].

Kruse [27] proposed a mathematical Eq. (1) for finding the Aerosol/Mie scattering attenuation coefficient ( $\beta_{as}(\lambda)$ ) at a particular wavelength.

$$\beta_{as}(\lambda) = \frac{3.912}{V_f} \left( \frac{\lambda}{550 \text{ (nm)}} \right)^{-q} \quad (1)$$

In the Eq. (1)  $q$  represents the scattering particle size distribution and  $V_f$  stands for visibility in m. The value of  $q$  is varying according to visibility, which is represented by Eq. (2).

$$q = \begin{cases} 1.6 & V_f > 50000 \text{ m} \\ 1.3 & 6000 \text{ m} < V_f < 50000 \text{ m} \\ 58.5 \times 10^{-2} V_f^{1/3} & V_f < 6000 \text{ m} \end{cases} \quad (2)$$

In the Kruse [27] model, size of particles is considered small in comparison to wavelength. So, Kim [25] modified this model according to the requirement, which is represented by Eq. (3).

$$q = \begin{cases} 1.6 & V_f > 50000 \text{ m} \\ 1.3 & 6000 \text{ m} < V_f < 50000 \text{ m} \\ 0.16 V_f + 0.34 & 1000 \text{ m} < V_f < 6000 \text{ m} \\ V_f - 0.5 & 500 \text{ m} < V_f < 1000 \text{ m} \\ 0 & V_f < 500 \text{ m} \end{cases} \quad (3)$$

This paper uses the Kim model [25] to find the attenuation under foggy environmental conditions. Moreover, under rainy conditions attenuation is calculated by Eq. (4) [26].

$$Y_{rain} = \begin{cases} 0.509R^{0.63} & R < 3.8 \text{ km} \\ 0.319R^{0.63} & 3.8 \text{ km} < R < 7.6 \\ 0.163R^{0.63} & R > 7.6 \end{cases} \quad (4)$$

Where  $R$  represents rain intensity and  $Y_{rain}$  stands for attenuation of rainy conditions (dB per km).

The effectiveness of the FSO System is diminished as a result of these variables. Thus, the MIMO ( $8 \times 8$  beams) approach is used in this research. In this particular piece of study, the meteorological conditions in the channel were examined in great detail. This means that the attenuation in the channel is 0.065 dB/km, 9.64 dB/km and 22 dB/km in clear climatic, medium rain, and foggy conditions, respectively. Finally, this optical signal is received by the FSO receiver (FSO Rx) module.

## 2.3 Receiving Section

In the Receiver part, PC ( $8 \times 1$ ) combines the output of FSO Rx modules. In addition to that, the WDM DEMUX is necessary for demultiplexing this signal. This signal is turned into 32 output signals by WDM DEMUX. The selector ( $32 \times 1$ ) is then used to choose which signal to send out. This separated signal is detected by a PD and filtered by an LPF. PIN PD and Bessel LPF are used for detecting light and filtering it. 3RG component regenerates an electrical signal. In the last section, the performance metrics are looked at with the help of measuring tools like the BER tester.

## 2.4 Closed-form Expression Of The BER For MIMO FSO System

In the FSO system receiver irradiance is modelled as  $I = I_l I_{at} I_p$ , where  $I$  is channel state,  $I_l$  represents the path loss,  $I_{at}$  accounts for the turbulence-induced fading and  $I_p$  signifies the impact of the pointing error impairment. The probability density function (PDF) of the pointing error impairment effect is given by Eq. (5) [28]:

$$f_{I_p}(I_p) = \frac{\xi^2}{A_0^{\xi^2}} I_p^{\xi^2-1}, 0 \leq I_p \leq A_0 \tag{5}$$

Where  $A_0$  represents the fraction of power collected at the receiver,  $\xi = B_0/2\sigma_s^2$  often referred to as ‘‘jitter,’’ is defined as the ratio of the equivalent beamwidth to the standard deviation of the pointing error displacement.

The PDF for the Gamma-Gamma turbulence model is given by Eq. (6) [29]:

$$f_{I_{at}}(I_{at}) = \frac{2(\alpha\beta)^{\frac{\alpha+\beta}{2}}}{\Gamma(\alpha)\Gamma(\beta)} I_{at}^{\left(\frac{\alpha+\beta}{2}\right)-1} K_{\alpha-\beta}\left(2\sqrt{\alpha\beta I_{at}}\right) \tag{6}$$

where  $K_{\alpha-\beta}(\dots)$  denotes the modified Bessel function of the second kind.  $\alpha$  and  $\beta$  stand for the count of small- and large-scale eddies, respectively. The values of  $\alpha$  and  $\beta$  are determined using Eq. (7a), Eq. (7b) respectively:

$$\alpha = \left[ \exp\left(\frac{0.49\sigma_v^2}{(1 + 1.11\sigma_v^{12/5})^{7/6}}\right) - 1 \right]^{-1} \tag{7a}$$

$$\beta = \left[ \exp\left(\frac{0.51\sigma_v^2}{(1 + 0.69\sigma_v^{12/5})^{5/6}}\right) - 1 \right]^{-1} \tag{7b}$$

$\sigma_v^2$  represents the Rytov variance, which serves as an indicator of the turbulence strength in the channel. The value of  $\sigma_v^2$  is determined through the use of Eq. (8):

$$\sigma_v^2 = 1.23c_n^2 k^{7/6} L^{11/6} \tag{8}$$

$c_n^2$  represents the refractive index structure parameter, and its values vary depending on the strength of atmospheric turbulence,  $k$  is wave number and  $L$  is link distance.

Now, the combined PDF of  $I = I_l I_{at} I_p$  is given by Eq. (9) [29]:

$$f_I(I) = \int f_{I/I_{at}}(I/I_{at}) f_{I_{at}}(I_{at}) dI_{at} \tag{9}$$

where  $f_{I/I_{at}}(I/I_{at})$  is defined as:

$$f_{I/I_p}(I/I_{at}) = \frac{1}{I_l I_{at}} f_{I_p}\left(\frac{I}{I_l I_{at}}\right) \tag{10}$$

Using Eq. (14) of [30], we can express the modified Bessel function of the second kind of Eq. (6) by utilizing Meijer’s G-function. Furthermore, by utilizing the argument simplification formula from Eq. (07.34.16.0001.01) of [31], we combine Eq. (5), Eq. (6), and Eq. (9) for obtain combined irradiance of the channel as given in Eq. (11).



$$f_I(I) = \int_{\frac{I}{A_0 I_l}}^{\infty} \frac{\xi^2 I^{\xi^2-1} (\alpha\beta)^{\frac{\alpha+\beta}{2}}}{(A_0 I_l)^{\xi^2} \Gamma(\alpha) \Gamma(\beta)} I_{at}^{\left(\frac{\alpha+\beta}{2}\right)-\xi^2-1} G_{0,2}^{2,0} \left[ \alpha\beta I_{at} \left| \frac{-}{2}, \frac{\beta-\alpha}{2} \right. \right] dI_{at} \tag{11}$$

where  $G_{p,q}^{m,n} [\cdot]$  denotes the Meijer’s G-function [30].

Now, simplifying Eq. (11), using the Meijer’s G-function translation formula [31], we get:

$$f_I(I) = \frac{\xi^2 \alpha \beta}{(A_0 I_l) \Gamma(\alpha) \Gamma(\beta)} G_{1,3}^{3,0} \left[ \frac{\alpha \beta I}{(A_0 I_l)} \left| \xi^2 - 1, \alpha - 1, \beta - 1 \right. \right] \tag{12}$$

The cumulative distribution function (CDF) is Eq. (12) is given by Eq. (13):

$$F_I(I) = \frac{\xi^2}{\Gamma(\alpha) \Gamma(\beta)} G_{2,4}^{3,1} \left[ \frac{\alpha \beta I}{(A_0 I_l)} \left| 1, 1 + \xi^2 \right. \right] \tag{13}$$

For the single channel (SC) FSO system average bit error probability can be calculated by averaging conditional error probabilities across the PDF of the instantaneous signal-to-noise ratio (SNR) [29].

$$P_{e,SC} = \int_0^{\infty} P_{e,SC}(I) f_I(I) dI \tag{14}$$

$$P_{e,SC}(I) = \frac{1}{2} \text{erfc} \left( \sqrt{\frac{SNR}{2}} \right) \tag{15}$$

where  $\text{erfc}(\bullet)$  represents the complementary error function and it is calculated by in terms of Gaussian Q(.) function  $2Q\sqrt{2\Phi} = \text{erfc}(\Phi)$ .  $P_{e,SC}(I)$  is the conditional BER probability for single FSO link. The expression for SNR is represented by Eq. (16).

$$SNR = \frac{(\gamma I)^2}{2\sigma^2} \tag{16}$$

where  $\gamma$  denotes responsivity of the photodetector and  $\sigma^2$  represents the variance of channel noise.

From Eq. (15) and Eq. (16) we get the expression of conditional BER probability:

$$P_{e,SC}(I) = \frac{1}{2} \text{erfc} \left( \sqrt{\frac{I\gamma}{2\sigma}} \right) \tag{17}$$

Subsequently, the ABER can be computed by applying Eqs. (17) and (12) in Eq. (14) and that is:

$$P_{e,SC} = \frac{\xi^2 \alpha \beta}{(A_0 I_l) \Gamma(\alpha) \Gamma(\beta)} \int_0^\infty \frac{1}{2} \operatorname{erfc} \left( \sqrt{\frac{I \gamma}{2\sigma}} \right) G_{1,3}^{3,0} \left[ \frac{\alpha \beta I}{(A_0 I_l)} \left| \begin{matrix} \xi^2 \\ \xi^2 - 1, \alpha - 1, \beta - 1 \end{matrix} \right. \right] dI \quad (18)$$

with the help of Eq. (8.4.14.2) of [32] we can represent the  $\operatorname{erfc}(\cdot)$  as a Meijer G-function. Additionally, from Eq. (21) of [30] we get the expression of ABER in the case of single channel FSO system:

$$P_{e,SC} = \frac{2^{\alpha+\beta-4} \xi^2}{\pi^{3/2} \Gamma(\alpha) \Gamma(\beta)} G_{7,4}^{2,6} \left[ \frac{4\gamma^2 A_0^2 I_l^2}{\sigma^2 \alpha^2 \beta^2} \left| \begin{matrix} \frac{1-\xi^2}{2}, \frac{2-\xi^2}{2}, \frac{1-\alpha}{2}, \frac{2-\alpha}{2}, \frac{1-\beta}{2}, \frac{2-\beta}{2}, 1 \\ 0, \frac{1}{2}, \frac{-\xi^2}{2}, \frac{1-\xi^2}{2} \end{matrix} \right. \right] \quad (19)$$

In our suggested system, we have implemented MIMO techniques within the communication channel. The current model involves X transmitting apertures and Y receiving apertures. The receiver irradiance in the case of MIMO system is modelled as  $I_{xy} = I_{l_{xy}} I_{at_{xy}} I_{p_{xy}}$ , where  $I_{xy}$  represents irradiance from the  $x^{\text{th}}$  transmitter and  $y^{\text{th}}$  receiver,  $I_{l_{xy}}$  relates the path loss, while  $I_{at_{xy}}$  correlates to atmospheric turbulence and  $I_{p_{xy}}$  accounts for pointing errors. The PDF of the suggested MIMO systems is represented using the Meijer G-function as

$$f_{I_{xy}}(I_{xy}) = \frac{\xi_{xy}^2 \alpha_{xy} \beta_{xy}}{(A_{0_{xy}} I_{l_{xy}}) \Gamma(\alpha_{xy}) \Gamma(\beta_{xy})} G_{1,3}^{3,0} \left[ \frac{\alpha_{xy} \beta_{xy} I_{l_{xy}}}{A_{0_{xy}} I_{l_{xy}}} \left| \begin{matrix} \xi_{xy}^2 \\ \xi_{xy}^2 - 1, \alpha_{xy} - 1, \beta_{xy} - 1 \end{matrix} \right. \right] \quad (20)$$

The ABER for MIMO links can be computed by Eq. (21) [33]:

$$P_{e,MIMO} = \int_0^\infty f_I(\mathbf{I}) \frac{1}{2} \operatorname{erfc} \left( \frac{h\gamma}{2XY\sigma} \sqrt{\sum_{x=1}^X \left( \sum_{y=1}^Y I_{xy} \right)^2} \right) dI \quad (21)$$

where  $f_I(\mathbf{I})$  represents joint PDF of vector  $\mathbf{I} = (I_{11}, I_{12}, I_{13}, \dots, I_{XY})$  of length XY.

By replacing the expression from Eq. (20) into Eq. (21), we obtain Eq. (22):

$$P_{e,MIMO} = \frac{\xi_{xy}^2 \alpha_{xy} \beta_{xy}}{A_{0_{xy}} I_{l_{xy}} \Gamma(\alpha_{xy}) \Gamma(\beta_{xy})} \int_0^\infty f_I(I) \frac{1}{2} \operatorname{erfc} \left( \frac{I \gamma}{2XY\sigma} \sqrt{\sum_{x=1}^X \left( \sum_{y=1}^Y I_{xy} \right)^2} \right) \times G_{1,3}^{3,0} \left[ \frac{\alpha_{xy} \beta_{xy} I_{l_{xy}}}{A_{0_{xy}} I_{l_{xy}}} \left| \begin{matrix} \xi_{xy}^2 \\ \xi_{xy}^2 - 1, \alpha_{xy} - 1, \beta_{xy} - 1 \end{matrix} \right. \right] dI_{xy} \quad (22)$$

By representing the  $\operatorname{erfc}(\cdot)$  as a Meijer G-function with the help of [Eq. (8.4.14.2)] of [32] and [Eq. (21)] of [30], the closed-form of BER of the proposed system given by Eq. (23):

$$P_{e,MIMO} = \prod_{x=1}^X \prod_{y=1}^Y \frac{2^{\alpha_{xy}+\beta_{xy}-4} \xi_{xy}^2}{\pi^{3/2} \Gamma(\alpha_{xy}) \Gamma(\beta_{xy})} \times G_{7,4}^{2,6} \left[ \frac{4\gamma^2 A_0^2 I_{l_{xy}}^2}{\alpha_{xy}^2 \beta_{xy}^2 X^2 Y^2} \left| \begin{matrix} \frac{1-\xi_{xy}^2}{2}, \frac{2-\xi_{xy}^2}{2}, \frac{1-\alpha_{xy}}{2}, \frac{2-\alpha_{xy}}{2}, \frac{1-\beta_{xy}}{2}, \frac{2-\beta_{xy}}{2}, 1 \\ 0, \frac{1}{2}, \frac{-\xi_{xy}^2}{2}, \frac{1-\xi_{xy}^2}{2} \end{matrix} \right. \right] \quad (23)$$

Equation (23) can be written in the SNR form by Eq. (24):

$$P_{e,MIMO} = \prod_{x=1}^X \prod_{y=1}^Y \frac{2^{\alpha_{xy}+\beta_{xy}-4} \xi_{xy}^2}{\pi^{3/2} \Gamma(\alpha_{xy}) \Gamma(\beta_{xy})} \times G_{7,4}^{2,6} \left[ \frac{8SNRA_0^2 I_{l_{xy}}^2}{\alpha_{xy}^2 \beta_{xy}^2 X^2 Y^2} \left| \begin{matrix} \frac{1-\xi_{xy}^2}{2}, \frac{2-\xi_{xy}^2}{2}, \frac{1-\alpha_{xy}}{2}, \frac{2-\alpha_{xy}}{2}, \frac{1-\beta_{xy}}{2}, \frac{2-\beta_{xy}}{2}, 1 \\ 0, \frac{1}{2}, \frac{-\xi_{xy}^2}{2}, \frac{1-\xi_{xy}^2}{2} \end{matrix} \right. \right] \quad (24)$$

We have used  $8 \times 8$  MIMO system in the channel part, so we can take the value of  $X=8$  and  $Y=8$ :

$$P_{e,MIMO} = \prod_{x=1}^8 \prod_{y=1}^8 \frac{2^{\alpha_{xy} + \beta_{xy} - 4} \xi_{xy}^2}{\pi^{3/2} \Gamma(\alpha_{xy}) \Gamma(\beta_{xy})} \times G_{7,4}^{2,6} \left[ \frac{1.9 \times 10^{-3} SNRA_{0xy}^2}{\alpha_{xy}^2 \beta_{xy}^2} \left| \begin{matrix} \frac{1-\xi_{xy}^2}{2}, \frac{2-\xi_{xy}^2}{2}, \frac{1-\alpha_{xy}}{2}, \frac{2-\alpha_{xy}}{2}, \frac{1-\beta_{xy}}{2}, \frac{2-\beta_{xy}}{2}, 1 \\ 0, \frac{1}{2}, \frac{-\xi_{xy}^2}{2}, \frac{1-\xi_{xy}^2}{2} \end{matrix} \right. \right] \quad (25)$$

Equation (25) represent the expression of closed-form of BER of proposed system.

### 3 Proposed Framework Simulation Design

The system parameters, together with their values and units, are shown in Table 1. In addition, the system is optimized by the use of an SPO method. In terms of transmission range, the goal of this iterative optimization [34] is to get the highest possible Q Factor while simultaneously achieving the lowest possible BER.

Now, the smallest possible value of  $a^*$  is determined as Eqs. (26),

$$r(a^*) \leq r(a), \forall a \text{ near } a^* \quad (26)$$

Again, the maximum value of the point  $b^*$  is obtained as Eq. (27)

$$s(b^*) \leq s(b), \forall b \text{ near } b^* \quad (27)$$

By Combining Eq. (26) and Eq. (27), we get Eq. (28)

**Table 1** Parameters and their values for a proposed framework

Simulation Parameters	Values
Frequency of the CW laser	193.1 THz
Power of the CW laser	10 dBm
Number of Channel	32
Extinction ratio	30 dB
Bit rate corresponding to each channel	10 Gbps
Forward pump power of EDFA	100 mW
Forward pump wavelength of EDFA	980 nm
Backward pump wavelength of EDFA	980 nm
Core radius	2.2 $\mu\text{m}$
Er doping radius	2.2 $\mu\text{m}$
Er metastable lifetime	10 ms
Numerical aperture	0.24
Er ion density	$10^{25} \text{ m}^{-3}$
Loss at 1550 nm	0.1 dB/m
Loss at 980 nm	0.15 dB/m
Length	5 m
Attenuation in clear climatic conditions	0.065 dB/km [21]
Attenuation in fog condition	22 dB/km [13]
Attenuation in medium rain condition	9.64 dB/km [13]
FSO Tx aperture Diameter	10 cm [23]
FSO Rx aperture Diameter	20 cm [35]
Divergence of the beam	2 mrad
Transmission Range	0–40 km
Responsivity	1 A/W
Dark Current	10 nA

$$t(ab) = \frac{r(a)}{s(b)} \tag{28}$$

So, maximizing  $t$ , we get Eq. (28):

$$Max.t(ab) = \frac{max.r(a)}{min.s(b)} \tag{29}$$

Equation (29) is validated only the condition of Eq. (30) will be fulfill.:

$$Subjected : \begin{cases} v \geq v_c \\ w \leq w_d \end{cases} \tag{30}$$

Here  $v$  stands for the data rate and  $w$  for the BER. It is important that the value of  $v$  must not be lower than  $v_c$ , and it is also necessary to ensure that the value of  $w$  must not be higher than  $w_d$ . Both  $v_c$  and  $w_d$ . are regarded as the typical values for a trustworthy optical communication system.

The simulation schematic layout of the proposed PRE, POST and PREPOST-amplification-based multiple beam WDM FSO system is shown in Fig. 3(a), 3(b) and 3(c), respectively.

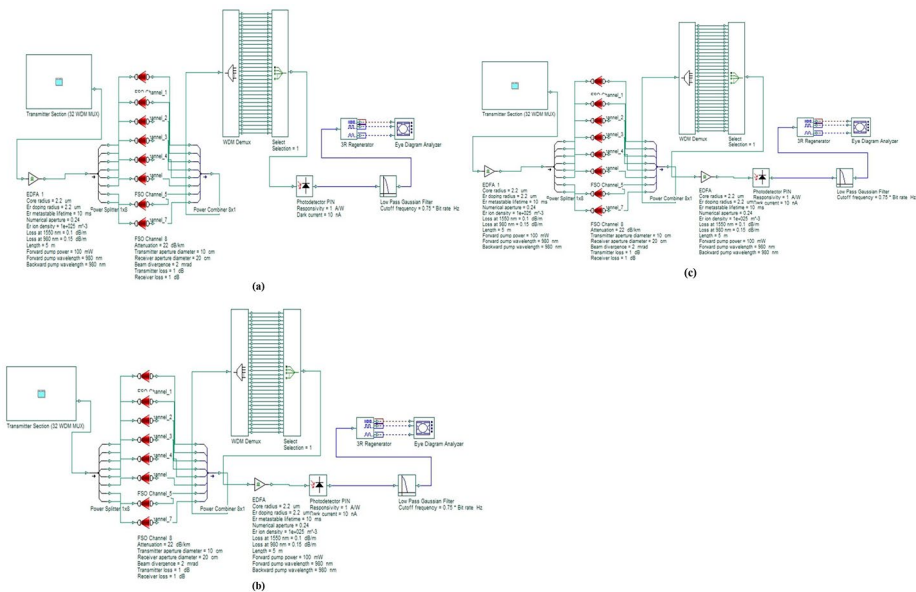


**Fig. 3** Simulation schematic layout of the proposed PRE, POST and PREPOST-amplification-based multiple beam WDM FSO system. **(a)** PRE-amplification approach **(b)** POST-amplification approach **(c)** PREPOST-amplification approach

## 4 Results and Discussion

In this section, we present a comparative analysis of the performance of different modulation schemes (RZ, NRZ, GA) combined with various amplification approaches (PREPOST, PRE, POST) under different climatic conditions with pointing error. For ease of reference, we use the following abbreviations to denote specific combinations of modulation schemes and amplification approaches:

“NRZ-PREPOST”: NRZ modulation scheme with a hybrid combination of PRE-POST- amplification approach.

“NRZ-PRE”: NRZ modulation scheme with a PRE-amplification approach.

“NRZ-POST”: NRZ modulation scheme with a POST-amplification approach.

“RZ-PREPOST”: RZ modulation scheme with a hybrid combination of PREPOST- amplification approach.

“RZ-PRE”: RZ modulation scheme with a PRE-amplification approach.

“RZ-POST”: RZ modulation scheme with a POST-amplification approach.

“GA-PREPOST”: GA modulation scheme with a hybrid combination of PREPOST- amplification approach.

“GA-PRE”: GA modulation scheme with a PRE-amplification approach.

“GA-POST”: GA modulation scheme with a POST-amplification approach.

### 4.1 Results Under Clear Climatic Conditions (Attenuation = 0.065 dB/km)

In clear climatic conditions, we evaluate the proposed approaches in terms of BER and Q Factor. Figure 4 illustrates the BER performance, and Fig. 5 depicts the Q Factor performance. Up to a transmission distance of 12 km, the RZ-PREPOST approach exhibits superior BER and Q Factor compared to other methods. Beyond this distance, the NRZ-PREPOST approach offers improved performance. Notably, the NRZ-PREPOST method achieves a maximum transmission range of 35 km with an acceptable BER.

**Fig. 4** BER evaluation of the suggested framework in clear climatic conditions

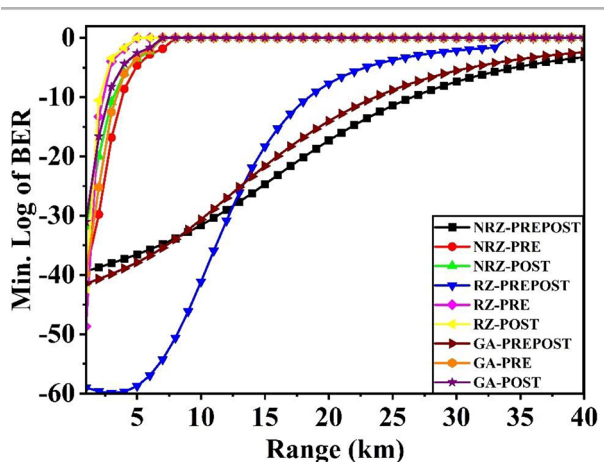


**Fig. 5** Q Factor evaluation of the suggested framework in clear climatic conditions

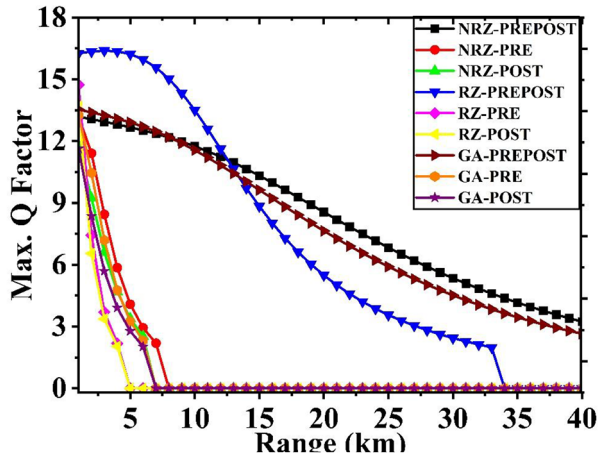
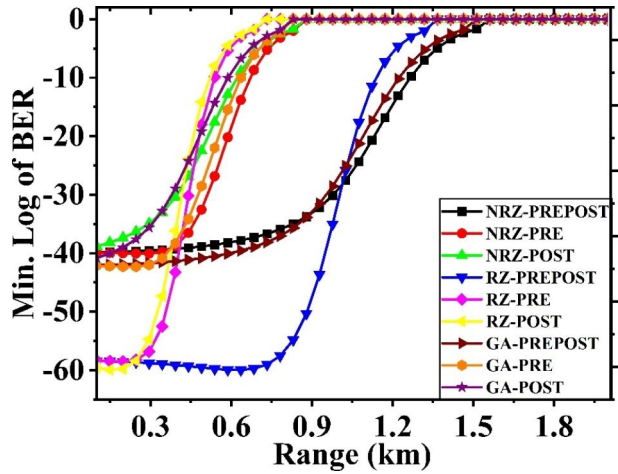


**Fig. 6** BER analysis of the proposed system in fog condition



**4.2 Results Under Foggy Conditions (Attenuation = 22 dB/km)**

Under foggy conditions, as shown in Figs. 6 and 7, the RZ-PREPOST approach continues to demonstrate favorable performance within the 1 km of transmission. Subsequently, the NRZ-PREPOST approach surpasses other techniques in terms of both BER and Q Factor. In this scenario, the maximum transmission range achieving the desired BER and Q Factor is 1.37 km.

**4.3 Results Under Medium Rainfall Conditions (Attenuation = 9.64 dB/km)**

For medium rainfall conditions, Figs. 8 and 9 depict the BER and Q Factor performance, respectively. The RZ-PREPOST approach excels up to a transmission distance of 1.72 km, after which the NRZ-PREPOST method offers improved Q Factor performance. Notably,

**Fig. 7** Q Factor analysis of the proposed system in fog condition

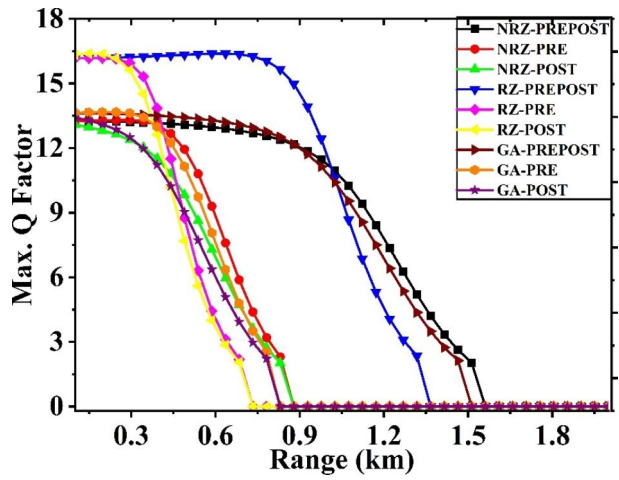


**Fig. 8** BER analysis of the proposed system in medium rain condition

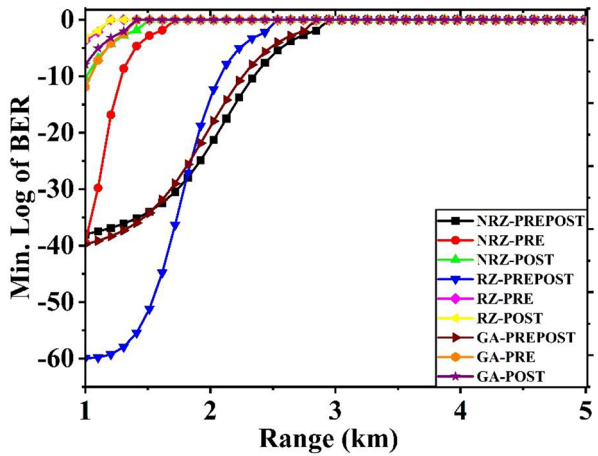


**Fig. 9** Q Factor analysis of the proposed system in medium rain condition

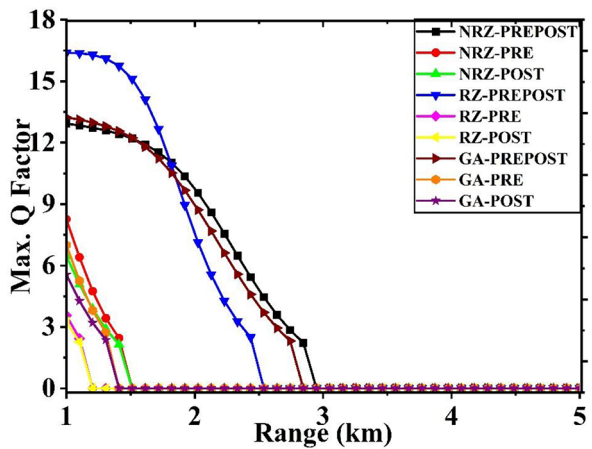


**Fig. 10** BER analysis of the proposed system in fog condition with pointing error

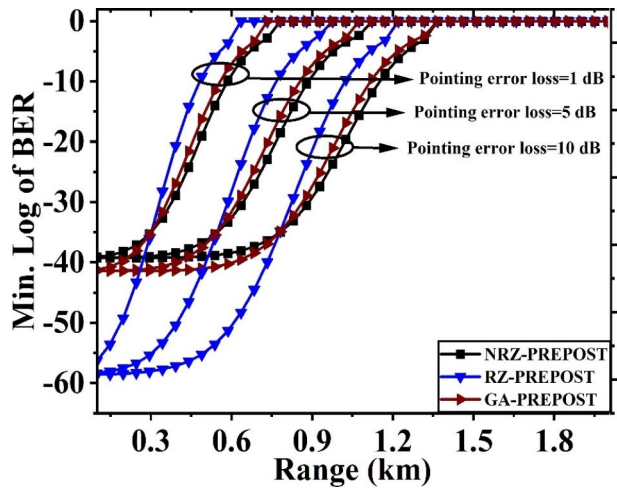
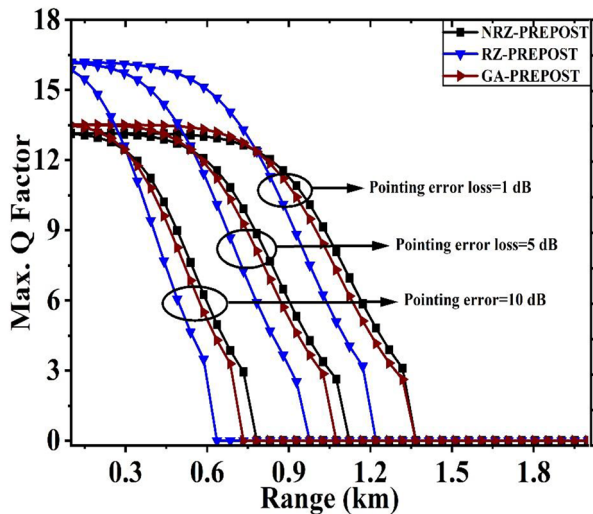


**Fig. 11** Q Factor analysis of the proposed system in fog condition with pointing error



the NRZ-PREPOST approach achieves a maximum transmission range of 2.53 km while maintaining an acceptable BER.

**4.4 Results Under Foggy Conditions (Attenuation = 22 dB/km) with Pointing Error**

Figures 10 and 11 provide insights into the effects of foggy conditions combined with pointing errors. Specifically, when a 1 dB loss resulting from pointing errors occurred at both the transmitter and receiver, the RZ-PREPOST approach consistently demonstrated commendable performance across a transmission distance of 782 m, after which the NRZ-PREPOST method offers improved BER, Q Factor performance. Notably, within this specific scenario, the NRZ-PREPOST strategy enabled an impressive maximum transmission range of 1.17 km while maintaining the prescribed benchmarks for BER and Q Factor. Furthermore,



**Fig. 12** BER analysis of the proposed system in medium rain condition with pointing error

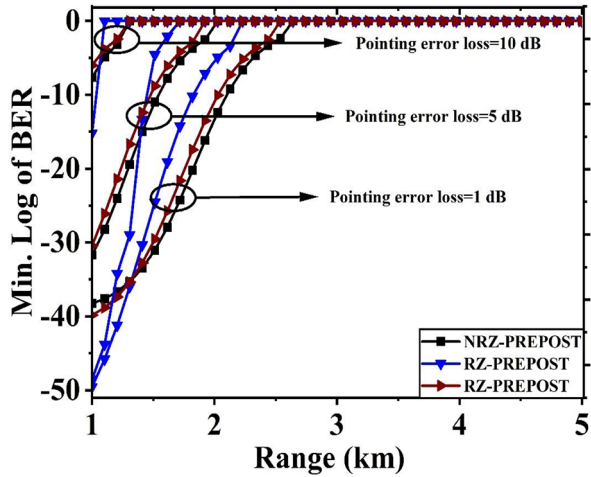
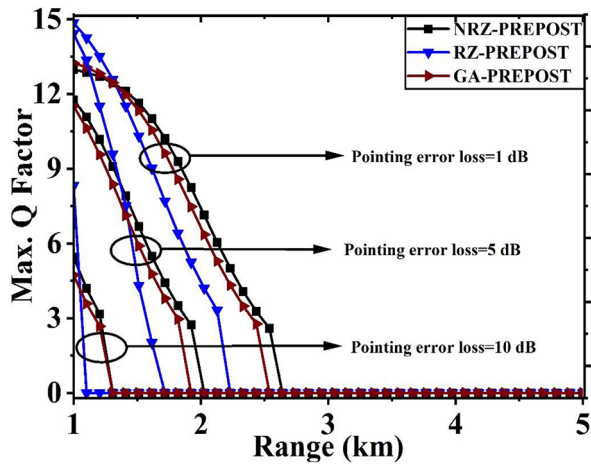


**Fig. 13** Q Factor analysis of the proposed system in in medium rain condition with pointing error



if the losses due to pointing errors were increased to 5 dB and 10 dB, the results indicated a reduction in the transmission range.

**4.5 Results Under Medium Rainfall Conditions (Attenuation = 9.64 dB/km) with Pointing Error**

Figures 12 and 13 provide insights into the impact of foggy conditions coupled with pointing errors. Specifically, when there was a 1 dB loss resulting from pointing errors at both the transmitter and receiver, the RZ-PREPOST approach consistently showcased commendable performance over a transmission distance of 1.3 km. Beyond this distance, the NRZ-PREPOST method demonstrated enhanced BER and Q Factor performance. Notably, within this specific scenario, the NRZ-PREPOST strategy enabled an impressive maximum transmission range of 2.23 km while maintaining the prescribed benchmarks for BER and Q

Factor. Furthermore, if the losses due to pointing errors were increased to 5 dB and 10 dB, the results indicated a reduction in the transmission range.

### 4.6 Comparative Assessment of The Proposed and Pre-existing Designs

Table 2 presents a comprehensive comparative analysis between the proposed framework and existing designs, shedding light on the framework’s superior performance across varying weather conditions. The proposed framework showcases its capability by achieving an impressive transmission range of 35 km under clear climatic conditions, a notable improvement over the previous designs limited to 25 km. Similarly, in rainy conditions, the proposed framework excels with a substantial transmission range of 2530 m, outperforming the previous designs that reached only 450 m. Similarly, the proposed framework attains a remarkable transmission range of 1370 m under foggy conditions, outshining the earlier design’s 500 m range. A distinguishing feature of the proposed framework is its reliance on the WDM-MIMO technique, setting it apart from the analyses conducted in [13], [17], [21], [24] and [36] which were based on SS-WDM, OAM, WDM-MIMO, WDM and MDM techniques, respectively. Noteworthy is the 10 Gbps data rate of each channel within the robust framework, collectively achieving an impressive channel capacity exceeding 320 Gbps. Importantly, the proposed design strategically employs EDFA amplification techniques, optimizes system parameters through the SPO technique; this was absent in previous studies. Moreover, the proposed system considers pointing error for simulation; Such consideration was lacking in prior investigations.

Eye diagrams of the proposed system under NRZ-PREPOST modulation schemes for foggy, rainy, and clear climatic conditions at a distance of 1 km are depicted in Figs. 14 and 15, and Fig. 16, respectively.

## 5 Conclusion

This study introduces a comprehensive strategy for addressing the impact of atmospheric conditions on FSO systems. The proposed MIMO WDM FSO system, incorporating pre- and post-amplification techniques, effectively achieves a substantial channel capacity of

**Table 2** Comparative examination of planned and existing designs

Parameters (Unit)	[13]	[17]	[21]	[24]	[36]	Proposed design
Transmission range under clear climatic condition (km)	1–5	-	25	3	2.5	35
Transmission range under rainy condition (m)	-	450	-	-	-	2530
Transmission range under foggy condition (m)	-	480	-	500	200	1370
Multiplexing technique	SS-WDM	OAM	WDM-MIMO	WDM	MDM	WDM-MIMO
Information rate (Gbps)	4 $\lambda \times 1.56$	4 $\lambda \times 10$	32 $\lambda \times 10$	8 $\lambda \times 10$	3 $\lambda \times 2.5$	32 $\lambda \times 10$
Amplifier used	✓ (EDFA)	✗	✗	✗	✗	✓ (EDFA)
Optimization used	✗	✗	✗	✓	✗	✓ (SPO)
Pointing error Considered	✗	✗	✗	✗	✗	✓

**Fig. 14** Eye diagram of the NRZ-PREPOST approach in foggy condition at 1 km

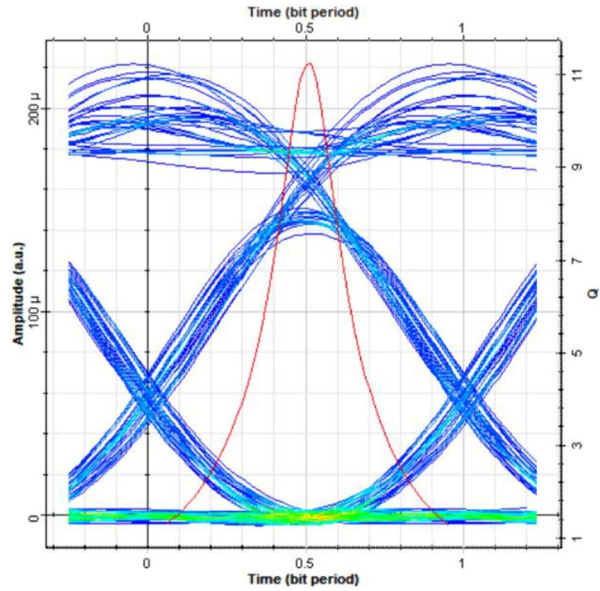
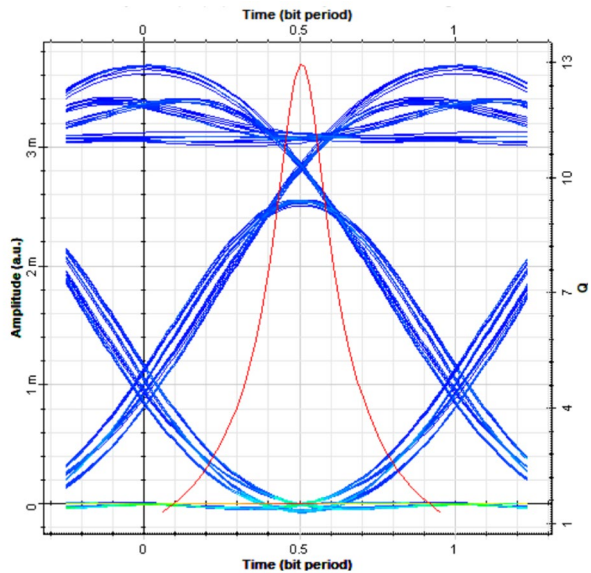
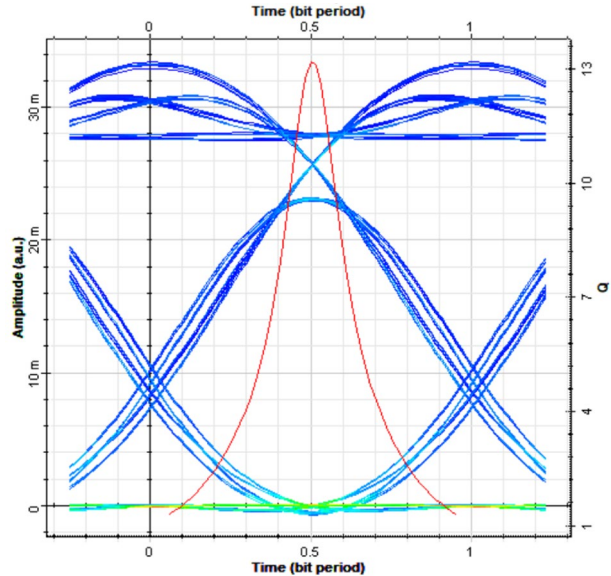


**Fig. 15** Eye diagram of the proposed system in rainy condition at 1 km



320 Gbps. Notably, the RZ-PREPOST approach demonstrates effectiveness within specific distance ranges under various climatic conditions, with the NRZ-PREPOST approach showcasing superior performance beyond those thresholds. A significant accomplishment lies in extending transmission ranges to 35 km in clear conditions, 1.37 km in foggy, and 2.53 km in rainy conditions. This innovative architecture holds great promise for future wireless communication networks, offering improved transmission range, channel capacity

**Fig. 16** Eye diagram of the proposed system in clear climatic condition at 1 km



and spectrum efficiency. An important application involves deploying the system in urban smart city networks, enabling cities to create high-capacity, low-latency communication connections for smart infrastructure elements. The proposed framework makes it easier to implement these, which include intelligent traffic management, environmental monitoring, public safety systems, and real-time data collection.

**Author Contributions** Yogesh Kumar Gupta: Conception and design, Manuscript preparation. Aditya Goel: Supervision and final approval.

**Funding** No funding.

**Data Availability** Not applicable.

## Declarations

**Conflict of Interest** Not Applicable.

**Ethical Approval** Not Applicable.

## References

1. Majumdar, A. K. (2015). *Advanced Free Space optics (FSO): A Systems Approach*. Springer.
2. Moll, F., Horwath, J., Shrestha, A., Brechtelsbauer, M., Fuchs, C., Navajas, L. A. M., & Díaz González, D. (2015). Demonstration of high-rate laser Communications from a fast Airborne platform. *IEEE Journal on Selected Areas in Communications*, 33(9), 1985–1995. <https://doi.org/10.1109/JSAC.2015.2433054>.
3. Kaushal, H., & Kaddoum, G. (2017). Optical Communication in Space: Challenges and Mitigation techniques. *IEEE Communications Surveys and Tutorials*, 19(1), 57–96. <https://doi.org/10.1109/COMST.2016.2603518>.

4. Seeds, A. J., Shams, H., Fice, M. J., & Renaud, C. C. (2015). TeraHertz photonics for wireless communications. *Journal of Lightwave Technology*, 33(3), 579–587. <https://doi.org/10.1109/JLT.2014.2355137>.
5. Hörack, G., Pezzei, P., Leitgeb, E., & Tischlinger, M. (2016). Alternative Broadband Network Connection for the Last Mile.
6. Banawan, M., Mishra, S. K., Gouin, A., Bacon, N., Guan, X., Wang, L., & Rusch, L. A. (2023). Using Standard 2×2 MIMO to increase capacity of spatial Multiplexing with OAM Modes. *Journal of Lightwave Technology*, 41(7), 1974–1984. <https://doi.org/10.1109/JLT.2022.3226628>.
7. Sridhar, B., Sridhar, S., & Nanchariah, V. (2022). Performance evaluation of FSO System under Atmospheric turbulence and noise. *Journal of the Institution of Engineers (India): Series B*, 103(6), 2085–2095. <https://doi.org/10.1007/s40031-022-00789-5>.
8. Bhatnagar, M. R., & Ghassemlooy, Z. (2016). Performance analysis of Gamma-Gamma Fading FSO MIMO links with pointing errors. *Journal of Lightwave Technology*, 34(9), 2158–2169. <https://doi.org/10.1109/JLT.2016.2526053>.
9. Nebuloni, R., & Verdugo, E. (2022). FSO path loss model based on the visibility. *IEEE Photonics Journal*, 14(2), <https://doi.org/10.1109/JPHOT.2022.3152728>.
10. Yu, X., Xu, G., Zhang, Q., & Song, Z. (2022). Dual-hop Optical Communication Systems over Málaga Turbulence under pointing error impairments with decode-and-Forward Protocol. *IEEE Photonics Journal*, 14(6), 1–15. <https://doi.org/10.1109/JPHOT.2022.3216283>.
11. Xu, G., Zhang, N., Xu, M., Xu, Z., Zhang, Q., & Song, Z. (2023). Outage probability and average BER of UAV-assisted dual-hop FSO Communication with Amplify-and-Forward relaying. *IEEE Transactions on Vehicular Technology*, 72(7), 8287–8302. <https://doi.org/10.1109/TVT.2023.3252822>.
12. Anuranjana, Kaur, S., Goyal, R., & Chaudhary, S. (2022). 1000 Gbps MDM-WDM FSO link employing DP-QPSK modulation scheme under the effect of fog. *Optik*, 257(March), 168809. <https://doi.org/10.1016/j.ijleo.2022.168809>.
13. Vasani, E., & Shah, V. (2023). Spectrum slicing-based performance analysis of Free Space Optical Communication under Atmospheric Turbulence. *Journal of the Institution of Engineers (India): Series B*, 104(1), 319–326. <https://doi.org/10.1007/s40031-022-00832-5>.
14. Singh, H., Miglani, R., Mittal, N., Gupta, S., Tubbal, F., Raad, R., & Amhoud, E. M. (2023). Designing an optimized free space optical (FSO) link for terrestrial commercial applications under turbulent channel conditions. *Optical and Quantum Electronics*, 55(6), 532. <https://doi.org/10.1007/s11082-023-04805-w>.
15. Vasani, E., & Shah, V. (2023). An Effective Design of Hybrid Spectrum Slicing WDM-PDM in FSO Communication System under different Weather Conditions. *Wireless Personal Communications*, 130, 777–800. <https://doi.org/10.1007/s11277-023-10309-3>.
16. Elsayed, E. E., Kakati, D., Singh, M., Grover, A., & Anand, G. (2022). Design and analysis of a dense wavelength-division multiplexed integrated PON-FSO system using modified OOK/DPPM modulation schemes over atmospheric turbulences. *Optical and Quantum Electronics*, 54(11), 1–27. <https://doi.org/10.1007/s11082-022-04142-4>.
17. Singh, M., Atieh, A., Grover, A., & Barukab, O. (2022). Performance analysis of 40 Gb/s free space optics transmission based on orbital angular momentum multiplexed beams. *Alexandria Engineering Journal*, 61(7), 5203–5212. <https://doi.org/10.1016/j.aej.2021.10.043>.
18. Mesri, L., & Djebbari, A. (2022). Performance limits of FSO based SAC-OCDMA system under Weather Conditions. *Journal of Optical Communications*, 43(2), 265–272. <https://doi.org/10.1515/joc-2018-0204>.
19. Singh, H., Mittal, N., Miglani, R., Singh, H., Gaba, G. S., & Hedabou, M. (2021). Design and analysis of high-speed Free Space Optical (FSO) Communication System for supporting Fifth Generation (5G) data services in diverse geographical locations of India. *IEEE Photonics Journal*, 13(5), 1–12. <https://doi.org/10.1109/JPHOT.2021.3113650>.
20. Shaker, F. K., & Ali, M. A. A. (2021). Multi-Beam Free-Space Optical Link to Mitigation of rain attenuation. *Journal of Optical Communications*, 42(2), 235–240. <https://doi.org/10.1515/joc-2018-0015>.
21. Rani, N., Singh, P., & Kaur, P. (2021). Mitigation of scintillation effects in WDM-FSO system using Homodyne detection. *Optik*, 248(October 2019), 168165. <https://doi.org/10.1016/j.ijleo.2021.168165>.
22. Gupta, Y. K., & Goel, A. (2023). Performance analysis of multiple-beam WDM free space laser-communication system using homodyne detection approach. *Heliyon*. <https://doi.org/10.1016/J.HELIYON.2023.E13325>. e13325.
23. Singh, M., & Malhotra, J. (2019). Performance investigation of high-speed FSO transmission system under the influence of different atmospheric conditions incorporating 3-D orthogonal modulation scheme. *Optical and Quantum Electronics*, 51(9), <https://doi.org/10.1007/s11082-019-1998-2>.

24. Badar, N., Jha, R. K., & Towfeeq, I. (2018). Performance analysis of an 80 (8 × 10) gbps RZ-DPSK based WDM-FSO system under combined effects of various weather conditions and atmospheric turbulence induced fading employing Gamma–Gamma fading model. *Optical and Quantum Electronics*, 50(1), 1–11. <https://doi.org/10.1007/s11082-017-1306-y>.
25. Kim, I. I., McArthur, B., & Korevaar, E. J. (2001). Comparison of laser beam propagation at 785 nm and 1550 nm in fog and haze for optical wireless communications. *Optical Wireless Communications III*, 4214, 26–37. <https://doi.org/10.1117/12.417512>.
26. Soni, G. (2018). Performance analysis of Free Space Optical Link under various attenuation Effects. *Science Journal of Circuits Systems and Signal Processing*, 7(2), 43. <https://doi.org/10.11648/j.cssp.20180702.11>.
27. Kruse, P. W., & McGlauchlin, L. D., R. B. M (1962). *Elements of Infrared Technology: Generation, transmission and detection*. Wiley.
28. Saw, B. K., Janyani, V., & Singh, G. (2023). Analysis of coherent-OFDM modulation for FSO communication over distribution with pointing errors. *Optics Communications*, 545(June), 129677. <https://doi.org/10.1016/j.optcom.2023.129677>.
29. Feng, J., & Zhao, X. (2017). Performance analysis of OOK-based FSO systems in Gamma–Gamma turbulence with imprecise channel models. *Optics Communications*, 402(March), 340–348. <https://doi.org/10.1016/j.optcom.2017.06.016>.
30. Adamchikand, V. S., & Marichev, O. I. (1990). The algorithm for calculating integrals of hypergeometric type functions and its realization in REDUCE system, 212–224. <https://doi.org/10.1145/96877.96930>. <http://functions.wolfram.com>.
31. Prudnikov, A. P., Brychkov, Y. A., & Mariche, O. I. (1986). *Integral and series, more special functions* (3 vol.). Gordon and Breach Science Publishers.
32. Tsiftsis, T. A., Sandalidis, H. G., Karagiannidis, G. K., & Uysal, M. (2009). Optical wireless links with spatial diversity over strong atmospheric turbulence channels. *IEEE Transactions on Wireless Communications*, 8(2), 951–957. <https://doi.org/10.1109/TWC.2009.071318>.
33. Lema, G. G. (2020). Free space optics communication system design using iterative optimization. *Journal of Optical Communications*, 000010151520200007. <https://doi.org/10.1515/joc-2020-0007>.
34. Ghalot, R., Madhu, C., Kaur, G., & Singh, P. (2019). Link estimation of different indian cities under Fog Weather Conditions. *Wireless Personal Communications*, 105(4), 1215–1234. <https://doi.org/10.1007/s11277-019-06142-2>.
35. Chaudhary, S., & Amphawan, A. (2018). Solid core PCF-based mode selector for MDM-Ro-FSO transmission systems. *Photonic Network Communications*, 36(2), 263–271. <https://doi.org/10.1007/s11107-018-0778-4>.

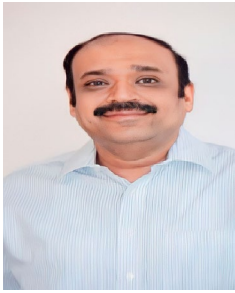
**Publisher's Note** Springer Nature remains neutral with regard to jurisdictional claims in published maps and institutional affiliations.

Springer Nature or its licensor (e.g. a society or other partner) holds exclusive rights to this article under a publishing agreement with the author(s) or other rightsholder(s); author self-archiving of the accepted manuscript version of this article is solely governed by the terms of such publishing agreement and applicable law.



**Yogesh Kumar Gupta** did his B.Tech. degree in Electronics and Communication Engineering in 2009 and later completed his M.Tech. degree from National Institute of Technology, Kurukshetra, in 2011. Currently, he is actively engaged in research within the Department of Electronics and Communication Engineering at the Maulana Azad National Institute of Technology, located in Bhopal, India. With 8 years of experience in academic roles within engineering institutes, his research encompasses several critical areas, including Free Space Optical Communication (FSO), wireless communication, high-capacity lightwave transmission systems, long-range Wavelength Division Multiplexing (WDM) networks, 5G technology, Multiple Input Multiple Output (MIMO) technology, and Machine Learning.





**Dr. Aditya Goel** did his B.E. (Hons) in Electronics & Communication from NIT Silchar and thereafter M.Tech. in Communication Engineering from I.I.T. Bombay. Subsequently he was awarded with the Ph.D. degree in Electronics & Communication Engineering in the Year 2000. He has rich teaching & research experience of more than 30 years in various cadres at Maulana Azad National Institute of Technology (MANIT), Bhopal. Presently he is working in the cadre of Professor in the Deptt. of Electronics & Communication Engineering at MANIT Bhopal since last 12 years (w.e.f 3/3/2010) and has worked as Chief Vigilance Officer (appointed by MHRD & CVC, Govt of India) of the Institute for a tenure of 3 years (2016–19) and has discharged various assignments related to the vigilance administration mainly comprising of Surveillance, Preventive & Punitive vigilance. He had also discharged his duties successfully as Professor & Head of the Department of Electronics & Comm.

Engineering, NIT Bhopal for a tenure of 2 years from Nov. 2011 to Nov. 2013. During his tenure as HOD, he performed various duties, significant among them were: Chairman Deptt U.G., Committee, Chairman Deptt. Post Graduate Committee, Chairman Deptt. Research Committee, Chairman Board of Studies. He was instrumental in development of various Labs of the Deptt for U.G & P.G Students. After that, he had also served as Dean (P&D) of the Institute and played a key role in planning the various policies pertaining to the overall development of the Institute. He has published more than 126 Research papers in reputed International Journals & Conferences including IEEE Journals. His areas of interests are Optical Communication, Digital Signal Processing, Optical Networks, Communication Engineering etc. He has successfully guided several M.Tech. dissertations and 13 Ph.D. thesis on these areas. He had been Principal Investigator of the research projects titled “Broadband Lightwave communication systems” and “High speed optical components for WDM systems” sanctioned by M.H.R.D. Govt. of India, New Delhi. He has also completed as Principal Investigator of another R&D Project “Broadband Multimedia Signal Processing and Applications” sanctioned by MANIT under grant in aid scheme of M.H.R.D. Govt. of India, New Delhi. He has published three patents in the area of Optical Communication at Patent office, Govt. of India, out of which two have been granted in April 2022 and Jan. 2023 and another one is in pipeline for award. He has reviewed many research papers of International conferences & journals including SPIE and IEEE. He has also been the reviewer of R&D projects sanctioned by DST, Govt. of India. He is a Life Fellow member of the Institution of Electronics & Telecommunication Engineers (IETE), Life Fellow member of Institution of Engineers (IE), and Senior Member of Computer Society of India (CSI). He had also served as Hon Secretary of Institution of Electronics & Telecommunication Engineers (IETE), M.P. State centre for two tenure -: 2000–2001 & 2004–2006. He organized a National Conference on Broadband Communications & Technologies (NCBBC – 2013) on 22nd & 23rd August 2013 as Organizing Chairman. He has delivered Keynote and Expert Lectures in various reputed Conferences and workshops. He visited the USA in Aug. 2007 to present his 3 research papers at an International Symposium of SPIE held in San Diego, USA.